Ocean Dynamics (2017) 67:485–497
DOI 10.1007/s10236-017-1041-8

An examination of the rheology of flocculated clay suspensions

Jeremy Spearman[1]

Received: 30 December 2015 / Accepted: 16 February 2017 / Published online: 20 March 2017

Abstract A dense cohesive sediment suspension, sometimes referred to as fluid mud, is a thixotropic fluid with a true yield stress. Current rheological formulations struggle to reconcile the structural dynamics of cohesive sediment suspensions with the equilibrium behaviour of these suspensions across the range of concentrations and shear. This paper is concerned with establishing a rheological framework for the range of sediment concentrations from the yield point to Newtonian flow. The shear stress equation is based on floc fractal theory, put forward by Mills and Snabre (1988). This results in a Casson-like rheology equation. Additional structural dynamics is then added, using a theory on the self-similarity of clay suspensions proposed by Coussot (1995), giving an equation which has the ability to match the equilibrium and time-dependent viscous rheology of a wide range of suspensions of different concentration and mineralogy.

Keywords Clay suspension · Rheology · Flocculation · Rheological model · Structural dynamics · Self-similarity

1 Introduction

A dense cohesive sediment suspension, sometimes referred to as fluid mud, is a thixotropic fluid with a true yield stress (Berlamont et al. 1993; Toorman 1997). The rheological properties of mud characterise its resistance to flow, deformation and structural changes. They are important for the estimation of sensitivity to liquefaction and erodibility, damping of turbulence and the prediction of density currents and fluid mud flow (Berlamont et al. 1993). As such, these properties are particularly important for estuaries with high (several grammes per litre) sediment concentrations, for muddy beds or intertidal banks or which experience significant wave action, for the side slopes of muddy dredged channels and for the navigation response of vessels sailing in low underkeel clearance in muddy estuaries. This paper is concerned with improving the description of mud rheology, developing a framework for the rheology of dense clay suspensions based on the physics of flocculated suspensions. It will be seen that this results in an equation which includes both structural dynamics and the ability to match the equilibrium rheology of a wide range of suspensions of different concentration and mineralogy in the viscous regime.

The paper includes a brief description of the similarity that results from fractal nature of flocs, a description of the structural similarity of clay suspensions identified by Coussot (1995) and a description of the structural dynamics approach put forward by Worrall and Tuliani (1964), all of which form significant inputs to the model development. A brief review of rheological models is also included which will provide an explanation of motivation. The paper will then develop a rheological model based on the principles of flocculation using an approach by Mills and Snabre (1988). The resulting rheological model is compared with equilibrium data for different clays across a range of concentrations and is compared with step-up and step-down data for different sediment suspensions.

This article is part of the Topical Collection on the *13th International Conference on Cohesive Sediment Transport in Leuven, Belgium 7–11 September 2015*

Responsible Editor: Erik A Toorman

✉ Jeremy Spearman
j.spearman@hrwallingford.com

[1] HR Wallingford, Howbery Park, Wallingford, Oxon OX8 10BA, UK

2 The quasi-fractal nature of clay suspensions and formation of gels

The primary mineral components contributing to the cohesion of muds are clay minerals. Clays have a plate-like structure and generally have primary particles of diameter less than 2 μm. Cohesion arises through the combined efforts of both the electrostatic charging of the clay minerals (if they are suspended in saline water) and various biogenic long-chain polymer molecules (Gratiot and Manning 2008; Manning et al. 2011). In general, clay particles aggregate with each other to form clusters or flocs with an apparent fractal structure (Huang 1993; Khelifa and Hill 2006; Winterwerp and van Kesteren 2004; Xu and Dong 2016). To be a truly fractal structure, however, the flocs would have to share a similar average structure characterised by a stochastic fractal nature and be scale invariant or "self-similar". In practice, this is not strictly true, and the fractal dimension varies slowly with floc size in a manner that can reasonably be characterised by a power law with an exponent of the order of −0.1 (Maggi 2007; Markussen and Andersen 2013; Xu and Dong 2016). In common with these researchers, in this paper, we make use of relationships relating to floc structure which follow from the fractal approximation (Sect. 5), but we do not constrain the fractal dimension to be a constant.

The flocs immobilise part of the continuous phase (in our case, water) which (as discussed later) leads to an increase in the effective sediment volume and to an increase in viscosity (Quemada 1998; Genovese 2012; Willenbacher and Georgieva 2013). Under conditions promoting clustering or flocculation (e.g. increasing volume concentration), flocs will aggregate further to form still larger clusters. Above a critical volume fraction, which is typically much smaller than the maximum packing fraction, these floc clusters form a large interconnected macroscopic network (Van Olphen 1956; Pignon et al. 1998) which is also (approximately) fractal and self-similar (Quemada 1998; Bremer 1992; Genovese 2012). This space-filling network results in highly elastic gel-like behaviour and an apparent yield stress (Toorman 1997; Willenbacher and Georgieva 2013).

3 A very brief review of rheological models for shear-thinning clay suspensions

There are a variety of different rheological models, but these models are often unsatisfactory either because they only describe the rheology well over a limited range of shear or because they are unable to represent the thixotropic (time dependent) nature of rheology of sediment suspensions by incorporating structural dynamics. At the heart of the first of these problems is that in general, for small shear rates, the stress associated with mud suspensions varies non-linearly with shear rate, while for high shear, the stress varies increasingly linearly as the Newtonian state is approached (Coussot 1995). Linear models like the Bingham model ($\tau = \tau_0 + \eta_B\gamma$, η_B is a constant) perform well for higher shear (where as the shear becomes larger, the viscosity tends to a linear, increasingly Newtonian, relationship), while non-linear models like the power law ($\tau = m\gamma^n$, m and n are constants) or Herschel-Bulkley ($\tau = \tau_0 + m\gamma^n$) models tend to be better at lower shear (where in general, suspensions do not behave in a linear fashion). None of these models performs well across the range of shear and yield stress dynamics. More sophisticated models like the Cross model and the Carreau model provide a better fit of the rheological behaviour of shear-thinning substances over a larger range of shear but require more empirical parameters. The Cross model is given by

$$\frac{\eta - \eta_\infty}{\eta_0 - \eta_\infty} = \frac{1}{1 + m\gamma^n} \tag{1}$$

The Carreau model has the following form:

$$\frac{\eta - \eta_\infty}{\eta_0 - \eta_\infty} = \frac{1}{(1 + m\gamma^2)^{n/2}} \tag{2}$$

where η is the apparent viscosity, η_0 and η_∞ are viscosity as $\gamma \to 0$ and $\gamma \to \infty$, and m and n are constants, These models also do not provide a transition to near Newtonian conditions under high shear, instead tending to a power law. Some of these equations can be modified to include additional rheological phenomena such as the transition from static to dynamic yield stress (e.g. Toorman 1997; de Souza 2011).

In addition to these viscous models, in more recent years, there has been a significant vein of research which has examined Maxwell or Jeffreys type rheological models combining viscous with viscoelastic contributions to rheology (e.g. Dullaert and Mewis 2006; Blackwell 2013; de Souza and Thompson 2013; Armstrong et al. 2016). These more complex models have largely targeted, with some success, the solid/low-shear transition to better reproduce thixotropic phenomena such as avalanching and the evolution from static yield to dynamic yield stress, although the viscous regime component is often based around a relatively simple Bingham-like term (e.g. Dullaert and Mewis 2006). These models have started to be applied to large amplitude oscillatory shear flows which allow rheological investigations over a wide range of deformation amplitudes and timescales (Armstrong et al. 2016).

As for structural dynamics, the time dependence of rheology of clay suspensions in the literature has largely focused on Bingham (Worrall-Tuliani) rheology models (e.g. van Kessel 1996; Toorman 1997; Knoch and Malcherek 2011; Oberrecht and Wurpts 2014), although some examples exist of use of

other models (e.g. Armelin et al. 2006; Moller et al. 2009) as well as the more complex time dependence of the thixotropic elastoviscoplastic models mentioned above.

The vast majority of rheological models have been developed from a standpoint of being able to empirically reproduce rheological phenomena (rather than being developed from a purely physically based point of view). The more complex the model (allowing more phenomena to be described), the more empirical parameters required. The values of these empirical parameters are drawn from laboratory studies. From a view point of sediment transport modelling, where suspension concentrations (as well as shear) can vary hugely in time, these models are not fit for purpose since a very large amount of laboratory study is required to describe how the rheology may vary under the range of conditions at a given site. A more physically based approach, however, could reduce the extent of this empiricism. This paper moves some way towards this goal by drawing upon aspects of the physics inherent in the structure of flocculating clays.

4 Structural dynamics—the Worrall Tuliani approach

The time-dependent rheological behaviour of a dense cohesive sediment suspension is often approximated by the structural kinetics theory, based on the Worrall and Tuliani (1964) approach, in which the fluid is described as a non-ideal Bingham fluid and the yield stress is taken as a measure for the structural parameter (Toorman 1997). For a Bingham fluid in equilibrium (exposed to a constant shear rate for a sufficiently long time), the shear stress is given by (Worrall and Tuliani 1964; Toorman 1997)

$$\tau = \tau_0 + \mu_\infty \dot{\gamma} + \frac{c\dot{\gamma}}{1+\beta\dot{\gamma}} \tag{3}$$

where τ is the shear stress, τ_0 is the yield stress at equilibrium, γ is the shear rate, μ_∞ is the Newtonian viscosity of the suspension at high shear rate, is a constant, and β and c are constants. The time-dependent version of Eq. 1 is given by (Toorman 1997)

$$\tau = \lambda\tau_0 + (\mu_\infty + c\lambda + \beta\tau_0\lambda_e)\gamma \tag{4}$$

In this equation, the structural parameter C is a measure of the degree of structure in the suspension. The value of λ is taken to be 0 for the situation where the bonds between clay particles are fully broken (in the limit of high shear) and taken to be 1 for the situation where the clay is fully structured. Moore (1959) defined a rate equation (Eq. 5) which expresses the structural state as the net result of break-up and recovery of the structure. The rate of break-down was assumed by Moore to depend on the shear rate γ causing the deformation and on the fraction of links existing at any given instant, and therefore, the rate of break-down was defined to be $-b\lambda\gamma$. The rate of build-up was assumed to be proportional to the fraction of links remaining to be formed $a(1-\lambda)$ resulting in the form of the equation shown in Eq. 3.

$$\frac{d\lambda}{dt} = a(1-\lambda) - b\lambda\dot{\gamma} = -a\frac{1}{\lambda_e}(\lambda-\lambda_e) \tag{5}$$

where a and b are constants and λ has an equilibrium value of

$$\lambda_e = \frac{1}{1+\frac{b}{a}\dot{\gamma}} = \frac{1}{1+\beta\dot{\gamma}} \tag{6}$$

A modified version of the Moore equation of the time dependency of λ is used in this paper (though other formulations exist, e.g. Coussot et al. 2002; Møller et al. 2006; Alexandrou et al. 2009), and γ is replaced by γ^m, resulting in

$$\frac{d\lambda}{dt} = a(1-\lambda) - b\lambda\dot{\gamma}^m = -a\frac{1}{\lambda_e}(\lambda-\lambda_e) \text{where } \lambda_e = \frac{1}{1+\beta\dot{\gamma}^m} \tag{7}$$

The rate of convergence of the structural parameter has been observed to vary with different powers of m (e.g. Galindo-Rosale and Rubio-Hernández 2006; Hammadi et al. 2015; Bekkour et al. 2005), and Eq. 7 caters for this variation. The physical significance of m is that it allows the assumed rate of break-down of the links within the clay structure to vary in a non-linear fashion with the shear rate.

The Worrall-Tuliani approach (Eqs. 4 and 5) requires five empirical values for τ_0, μ_∞, c, β and a (Toorman 1997). However, in a time-varying cohesive sediment suspension, some of these empirical values vary depending on the sediment concentration.

5 Structural similarity of sediment suspensions

An important feature of the framework that will be introduced later in this paper is the idea that sediment suspensions are structurally similar. This idea was put forward by Coussot (1995) who showed experimentally that, in a wide solid fraction range, the behaviour of clay suspensions is similar and goes through a transition from non-Newtonian to Newtonian when a non-dimensional shear rate increases. An example is shown in Fig. 1 for a series of kaolin-water suspensions.

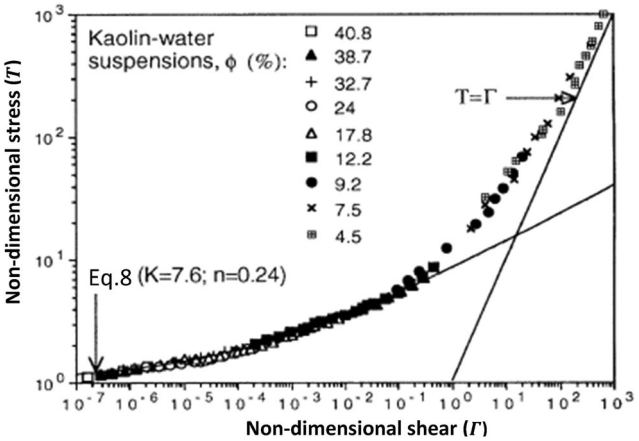

Fig. 1 Plot of non-dimensional stress against non-dimensional shear for kaolinite suspensions of varying concentration. Figure reproduced from Coussot (1995) with the permission of the American Physical Society

Coussot identified that the equilibrium shear and stress for low shear could be described by a power law involving non-dimensional values,

$$T = 1 + K\Gamma^n \tag{8}$$

where $T = \frac{\tau}{\tau_0}$, $\Gamma = \frac{\dot{\gamma}\mu_\infty}{\tau_0}$, and K and n are constants dependent on mineralogy but independent of concentration. For the two clay suspensions investigated, Coussot found K ~4.5–7.6 and n ~0.2–0.25.

6 Deriving a rheological model from physical principles associated with flocculation

6.1 Rheology under equilibrium conditions

Consider first a densely concentrated Newtonian suspension of hard spheres. The viscosity of the suspension is given by (Quemada 1977).

$$\frac{\mu}{\mu_0} = \frac{1}{\left(1-\phi/\phi^*\right)^2} \tag{9}$$

where μ is the viscosity of the suspension, μ_0 is the viscosity of the liquid phase, ϕ is the sediment volume concentration and ϕ^* is the maximum sediment volume concentration. Other equations similar to Eq. 9 can be used—for instance the Krieger and Dougherty (1959) equation or the Chong et al. (1971) equation, but Eq. 9 has the additional merit of simplifying the algebra.

Now consider a densely concentrated floc suspension. Under these conditions, the viscosity is a function of the *effective* sediment volume, ϕ_{eff} (Quemada 1998; Blachier et al. 2013; Willenbacher and Georgieva 2013). This is because some amount of suspending fluid is trapped within the floc structures and ϕ_{eff} is the sediment volume concentration which takes this into account. The equivalent of Eq. 5 for floc structures is given by Eq. 10

$$\frac{\mu}{\mu_0} = \frac{1}{\left(1-\phi_{eff}/\phi^*\right)^2} \tag{10}$$

We assume that the suspension is formed of flocs of fractal dimension D. The fractal dimension can be used to describe the effective volume concentration as follows (Mills and Snabre 1988; McClements 1999; Coupland and Sigfusson 2006; Metin and Bonnecaze 2014):

$$\phi_{eff} = \phi\left(\frac{R_F}{d}\right)^{3-D} \tag{11}$$

where R_F is the characteristic dimension of the floc structure and d is the dimension of the primary particles.

The focus of this paper is the application of Eq. 11 and the rheological model that results for dense concentrated suspensions beyond the gel point. For such dense cohesive suspensions, the suspension is a gel formed of an infinite cluster of fractal flocs, the characteristic dimension of which is R_F at equilibrium (Mills and Snabre 1988). The characteristic dimension R_F is governed by the balance between the shear forces acting to rupture and break down the flocs and by the inherent strength of the floc to resist this rupturing process. We use this idea with the method of Mills (1985) and Mills and Snabre (1988) to establish a relationship between R_F and the shear applied. To do this, we introduce a surface energy, , which represents the ability of the floc to resist break-up, and we equate this surface energy with the applied shear at the point of rupture. The energy required to rupture a flow consists of two parts: the energy to rupture the links which have been formed between the particles inside the floc and the energy to stretch (but not break) the elastic links between particles within the floc. Of these two parts, most of the energy dissipation is associated with the stretching processes rather than the rupture (Firth and Hunter 1976; Bache and Gregory 2007). It is necessary to characterise both these contributions.

We start with the stretching or deformation process. It can be shown that the energy required per unit area (the surface energy,) to stretch the bonds within a floc prior to rupturing scales is (Mills and Snabre 1988)

$$Z \propto \tau_D R_F \tag{12}$$

where τ_D is that part of the shear stress acting to stretch (deform) the floc bonds. The same result can be derived from the Firth and Hunter (1976) result that the total energy required to stretch bonds within floc scales is $E_{Tot} \propto F_D R_F$, (assuming that the energy dissipation due to fluid flowing into the space left by the stretching bonds between flocs is small compared to that from stretching of the bonds), and therefore, $Z \propto E_{Tot}/R_F^2 \propto \tau_D R_F$.

Now, we characterise the floc rupture. Derjaguin et al. equation (1975) gives the relationship between the force need to overcome the strength of the floc surface F_R and the surface energy as

$$F_R = 2\pi R_F Z \tag{13}$$

where F_R is the force necessary to cause rupture. But because the force acts over the surface of the floc, then $F_R \propto R_F^2$ τ_R (Snabre et al. 1987), where τ_R is the shear at the point of rupture. This gives the result

$$Z \propto \tau_R R_F \tag{14}$$

Since the total shear stress acting on the floc can be decomposed into the shear acting to cause elastic stretching and the shear acting to induce rupture, $\tau = \tau_R + \tau_D$. Both τ_R and τ_D scale as Z/R_F, so it must be true that the total stress contributing to floc break-up τ does so as well.

The surface energy in the section of rupture can also be defined in terms of the bond energy between primary particles. In this way, Z equals the product of the number of bonds (per unit area) and the bond energy between each bonding pair of particles. It is convenient to establish Z in terms of the total number of primary particles within the floc and the radii of primary particle and floc, but for the purposes of this derivation, it is not necessary to go into detail regarding the nature of the bonds themselves (Mills and Snabre 1988). The exact nature of the physicochemical interactions (van der Waals, electrostatic, bridging, etc) is hence deliberately ignored.

$$Z = \frac{N_{surf}\,\zeta a^2}{R^2} = N_{floc}\left(\frac{4\pi R_F^2 d}{\frac{4}{3}\pi R_F^3}\right)\frac{\zeta a^2}{R^2} = N_{floc}\left(\frac{3\zeta a^3}{R^3}\right) \tag{15}$$

where N_{surf} is the number of primary particles in the surface of the floc, N_{floc} is the total number of primary particles in the floc, and ζd^2 is the bond energy between every pair of particles with ζ an empirical parameter denoting bond energy strength. Equations 12, 14 and 15 lead, along with the definition of the fractal dimension, $N_{floc} = (R_F/d)^D$ (Maggi 2005), to the result

$$\frac{R_f}{d} = \left[\frac{A\tau^*}{\tau}\right]^{1/(4-D)} \tag{16}$$

where A is a constant related to floc break-up and $\tau^* = \frac{\zeta}{d}$ is a yield strength property related to the surface energy. Mills and Snabre (1988) note that in the limit, under high shear, $R_f \to d$ rather than zero and therefore Eq. 16 needs to be adapted as follows:

$$\frac{R_f}{d} - 1 = \left[\frac{A\tau^*}{\tau}\right]^{1/(4-D)} \tag{17}$$

We now combine Eqs. 7 and 13 and we get

$$\phi_{eff} = \phi\left[1 + \left(\frac{\lambda}{\lambda_e}\right)^{1/(4-D)}\left(\frac{A\tau^*}{\tau}\right)^{1/(4-D)}\right]^{3-D} \tag{18}$$

Inserting Eq. 18 into Eq. 10 gives

$$\left(\frac{\mu}{\mu_0}\right)^{\frac{1}{2}} = \frac{1}{\left\{(1-\phi/\phi^*)\left[1 + \left(\frac{\lambda}{\lambda_e}\right)^{\frac{1}{4-D}}\left(\frac{\phi/\phi^*}{(1-\phi/\phi^*)}\right)\left(\frac{A\tau^*}{\tau}\right)^{1/(4-D)}\right]^{3-D}\right\}} \tag{19}$$

or

$$\left(\frac{\mu}{\mu_\infty}\right)^{\frac{1}{2}} = \frac{1}{\left[1 + \left(\frac{\lambda}{\lambda_e}\right)^{\frac{1}{4-D}}\left(\frac{\tau_0}{\tau}\right)^{1/(4-D)}\right]^{3-D}} \tag{20}$$

where $\frac{\mu_\infty}{\mu_0} = \frac{1}{(1-\phi/\phi^*)^2}$ and

$$\tau_0 = \left[\frac{\phi/\phi^*}{(1-\phi/\phi^*)}\right]^{4-D}(A\tau^*) \tag{21}$$

Equations 20 and 21 lead to

$$\left[\tau^{\frac{1}{4-D}} - \left(\frac{\lambda}{\lambda_e}\right)^{\frac{1}{4-D}}\tau_0^{\frac{1}{4-D}}\right]^{3-D} = \left(\frac{\mu_\infty}{\mu}\right)^{1/2}\tau^{\left(\frac{3-D}{4-D}\right)} \tag{22}$$

This can be rewritten as

$$\tau^{\frac{1}{4-D}} = \left(\frac{\lambda}{\lambda_e}\right)^{\frac{1}{4-D}}\tau_0^{\frac{1}{4-D}} + \left(\mu_\infty \dot{\gamma}\right)^{\frac{1}{4-D}}\left(\frac{\mu}{\mu_\infty}\right)^{\epsilon} \quad \text{where } \epsilon = \frac{1}{4-D} - \frac{1}{2(3-D)} \tag{23}$$

We approximate $\left(\frac{\mu}{\mu_\infty}\right)$ by the equilibrium form of Eq. 20, into the right hand side of Eq. 23, which results in

$$\approx \left(\frac{\lambda}{\lambda_e}\right)^{\frac{1}{4-D}}\tau_0^{\frac{1}{4-D}} + (\mu_\infty \dot{\gamma})^{\frac{1}{4-D}} \times \left[1 - \left(\frac{3-D}{4-D} - \frac{1}{2}\right)\left(\frac{\tau_0}{\tau}\right)^{\frac{1}{4-D}}\right] \tag{24}$$

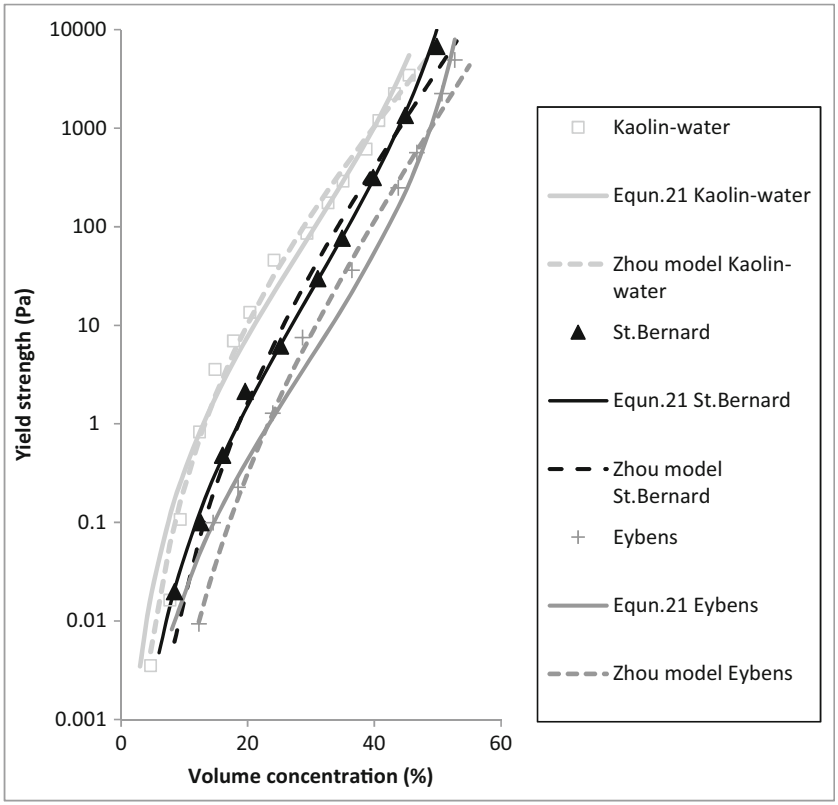

Fig. 2 Yield stress of the clay suspensions considered in this chapter. Data from Coussot (1995). Model predictions are from Eq. 21

In practice, the $\left(\frac{3-D}{4-D}-\frac{1}{2}\right)\left(\frac{\tau_0}{\tau}\right)^{\frac{1}{4-D}}$ term is small. Even when D is close to 3 and τ is close to τ_0, then γ is small and the contribution of this term to τ is small. Henceforth, we will assume that this term can be ignored. When D is equal to 2, then at equilibrium, Eq. 22 becomes equal to Casson's equation.

As indicated in Worrall and Tuliani (1964) and Toorman (1997), an additional term $f(\lambda)$ needs to be added to Eq. 24 to account for the effect of structural dynamics on the shear rate term, i.e.

$$\tau^{\frac{1}{4-D}} = \left(\frac{\lambda}{\lambda_e}\right)^{\frac{1}{4-D}} \tau_0^{\frac{1}{4-D}} + \left\{1+f(\lambda)\right\}^{\frac{1}{4-D}} \left(\mu_\infty \dot{\gamma}\right)^{\frac{1}{4-D}} \tag{25}$$

Putting Eq. 25 in the same form as Eq. 8, we get

$$T^{\frac{1}{4-D}} = 1 + \left\{1+f(\lambda)\right\}^{\frac{1}{4-D}} \Gamma^{\frac{1}{4-D}} \Rightarrow T \approx 1 + (4-D)\left\{1+f(\lambda)\right\}^{\frac{1}{4-D}} \Gamma^{\frac{1}{4-D}} \text{ for small } \Gamma \tag{26}$$

In order for the equation to become equal to the power law found by Coussot (1995) for small Γ (see Fig. 1), $f(\lambda)$ has to be of the form $\left(\frac{\dot{\gamma}}{\gamma_0}\right)^{-m}$ for equilibrium conditions, where m is positive. This is satisfied by setting

$$f(\lambda) = \left(\frac{\lambda}{1-\lambda}\right)^m \left(\frac{\tau_0}{\mu_\infty}\right)^m \tag{27}$$

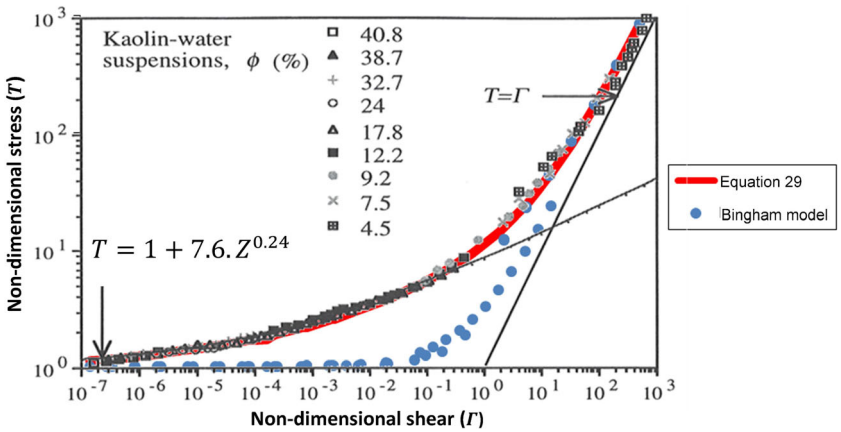

Fig. 3 Comparison of Eq. 29 (*red line*) with data for a kaolinite suspension (*black/grey symbols*). The best overall fit using a Bingham model is shown by the *blue circles*. Measured data from figure reproduced from Coussot (1995) with the permission of the American Physical Society

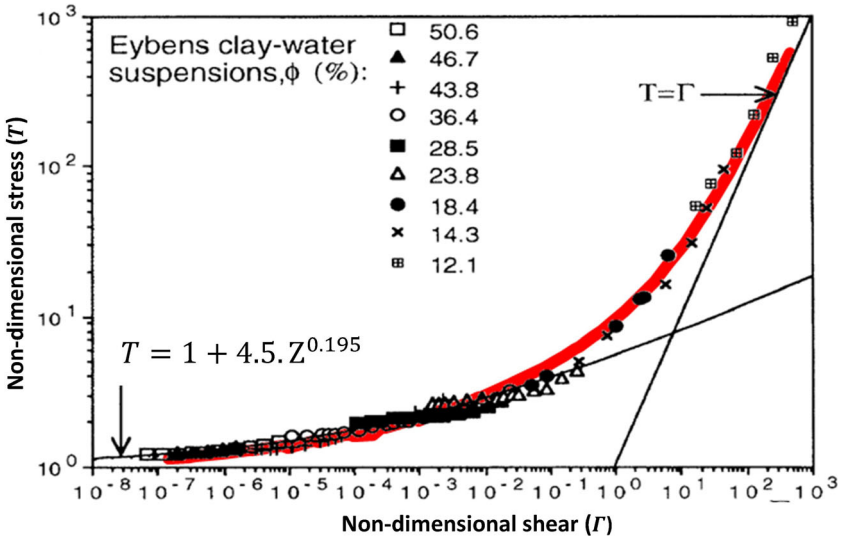

Fig. 4 Comparison of Eq. 29 (*red line*) with data for a St. Bernard clay suspension (*black symbols*). Figure reproduced from Coussot (1995) with the permission of the American Physical Society

where, as discussed in Sect. 4, the equilibrium value of the structural parameter λ is given by $\lambda_e = \frac{1}{1+\beta\dot{\gamma}^m}$. This gives the final form of the time-dependent and equilibrium equations as

$$\tau^{\frac{1}{4-D}} = \left(\frac{\lambda}{\lambda_e}\right)^{\frac{1}{4-D}} \tau_0^{\frac{1}{4-D}} + \left\{1 + \left(\frac{\tau_0}{\mu_\infty}\right)^m \left(\frac{\lambda}{1-\lambda}\right)^m\right\}^{\frac{1}{4-D}} \left(\mu_\infty \dot{\gamma}\right)^{\frac{1}{4-D}} \quad (28)$$

$$\tau^{\frac{1}{4-D}} = \tau_0^{\frac{1}{4-D}} + \left\{1 + \left(\frac{1}{\beta\dot{\gamma}^m}\right)\left(\frac{\tau_0}{\mu_\infty}\right)^m\right\}^{\frac{1}{4-D}} \left(\mu_\infty \dot{\gamma}\right)^{\frac{1}{4-D}} \quad (29)$$

7 Results

In this section, Eqs. 28 and 29 are applied to data for equilibrium and time-varying conditions. The equilibrium comparisons will show that Eq. 29 is able to describe the equilibrium rheology of a range of clays across the range from low to high shear and for a range of sediment volume concentrations from 5 to 50%. The comparisons of data under time-varying (step-up and step-down tests) will show that Eq. 28 is able to describe the time-varying rheology.

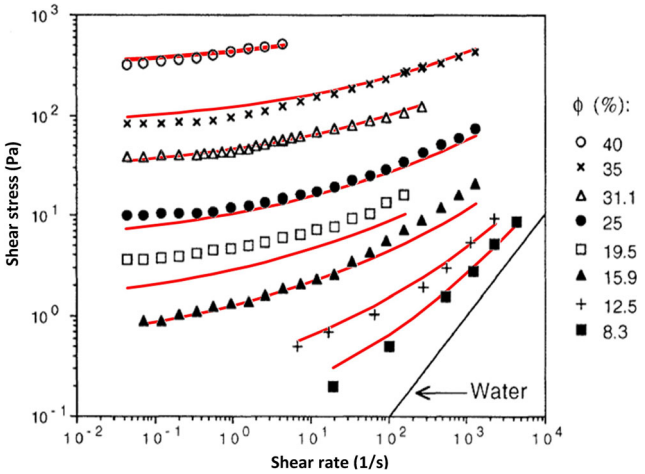

Fig. 5 Comparison of Eq. 29 (red line) with data for a Lake Eybens clay suspension (*black symbols*). Figure reproduced from Coussot (1995) with the permission of the American Physical Society

7.1 Equilibrium conditions—data from Coussot (1995)

For this set of comparisons, the data used for comparison with Eq. 29 is from Coussot (1995) and includes

- A natural kaolinite.
- A debris flow deposit from St. Bernard (French Alps), a mixture of chlorite and illite.
- A deposit from Lake Eybens (also French Alps), a mixture of chlorite and illite.

Coussot (1995) provides values of τ_0 for these three clays for a range of concentrations (Fig. 2). Although we use the values measured by Coussot in Figs. 3, 4 and 5, it is worthwhile examining the underlying assumptions used in the present model regarding the yield strength. Equation 21 gives the form of the yield strength with respect to volume concentration as $\tau_0 = k\left[\frac{\phi/\phi^*}{(1-\phi/\phi^*)}\right]^{2(4-D)}$ where $k = A\tau^*$ in Eq. 21 and

Table 1 Rheological constants used to fit Eq. 29 in Figs. 3, 4 and 5

Clay type	D	$1/(4-D)$	m	β
Kaolinite	2.3	0.60	0.62	0.17
Lake Eybens	2.3	0.60	0.72	0.5
St. Bernard	2.1	0.52	0.55	0.14

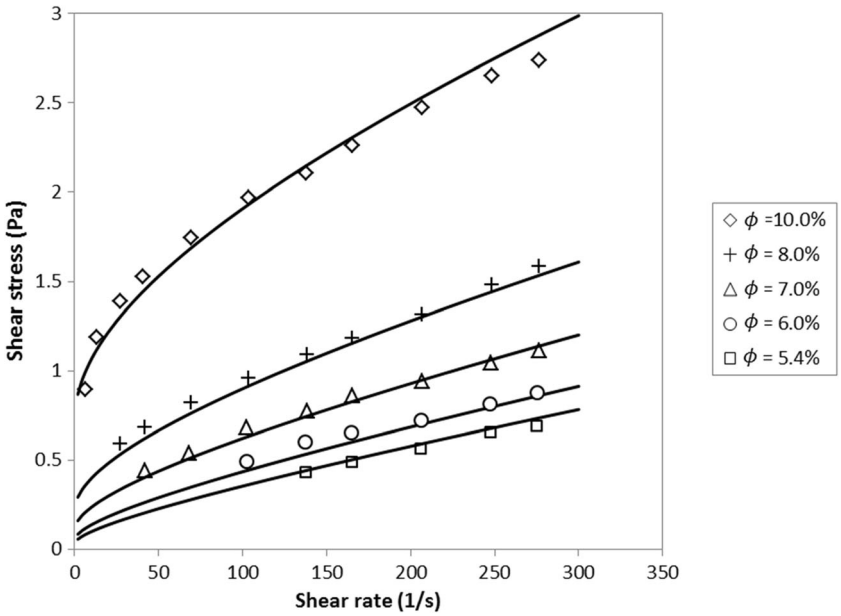

Fig. 6 Comparison of Eq. 29 (*continuous lines*) with data for a kaolin-water suspension (*symbols*). Data from Hendratta and Ohmoto (2012)

D is specified by the fit in Figs. 3, 4 and 5. Equation 21 is similar in form to equations given by Zhou et al. (1999), who found $\tau_0 = k'\left[\frac{\phi}{(1-\phi)}\right]^{c'} \times \frac{1}{d^2}$ where d is the particle diameter of the clay suspension. A comparison between the Zhou and Eq. 21 models is shown in Fig. 2. The Zhou model result is derived by treating k'/d^2 and c' as fitting parameters. This is compared with the Eq. 21 result where the only fitting parameter used is k (the exponent $2(4-D)$ being prescribed by the parameter fitting in Figs. 3, 4 and 5). Both model results are similar and fit the data well with Eq. 21 fitting the data better as ϕ tends to the maximum packing fraction (typically ≈0.6 for clays), while the Zhou model (aided by the greater degree of freedom resulting from two fitting parameters) fits the data better at low values of ϕ.

Application of Eq. 29 to the three different clays for equilibrium conditions is shown in Figs 3, 4 and 5. It can be seen that Eq. 29 fits the data well for the range of sediment concentrations and shear. It appears that the proposed model is able to predict the smooth transition between shear stress dominated by the yield stress to that dominated by the Newtonian viscosity. The relevant rheological constants achieved through calibration for these three applications of the equilibrium form of Eq. 29 are presented in Table 1. The values of μ_∞ were computed from Eq. 8 and so varied with volume concentration. The values of τ_0 were taken from the measurements of Coussot shown in Fig. 2. Note that the calibrated constants—the fractal dimension, D, the exponent, m, and the structural equilibrium parameter β—were valid for the whole of the spectrum of volume concentrations.

It should also be noted that the good fit achieved with Eq. 29 was not achieved with a best fit Bingham model with the Worrall-Tuliani structural dynamics (Eq. 3)—as shown in Fig. 3.

Table 2 Rheological constants used to fit Eq. 29 in Fig. 6

D	$1/(4-D)$	m	B	k (Eq. 21)
1.7	0.43	0.001	100	7.4

7.2 Equilibrium conditions—data from Hendratta and Ohmoto (2012)

For this set of comparisons, the data used is from Hendratta and Ohmoto (2012). This data set is composed of the rheological measurements of the shear stress of kaolin suspensions under equilibrium conditions, under different shear rates and at different sediment volume concentrations. The kaolin used had a median particle size diameter of 5.3 μm and was primarily composed of very fine silt (with <20% clay-sized particles).

Figure 6 shows the comparison of Eq. 29 with the Hendratta and Ohmoto data. The parameters used to fit the data are shown in Table 2. Figure 6 shows that Eq. 29 gives a reasonable fit across the range of shear rate and volume concentration based on only four parameters.

7.3 Step-up and step-down tests by Coussot (1993)

In this section, Eq. 28 is compared to the model against step-up and step-down shear experiments from Coussot (1993). The suspension used was bentonite-water mixture containing about 90% of montmorillonite with particle diameter below 2 μm and small percentages of kaolinite, illite and calcite. The bentonite was mixed with water (at a solid volume concentration of 4%) for 20 min and was left to rest for 24 h.

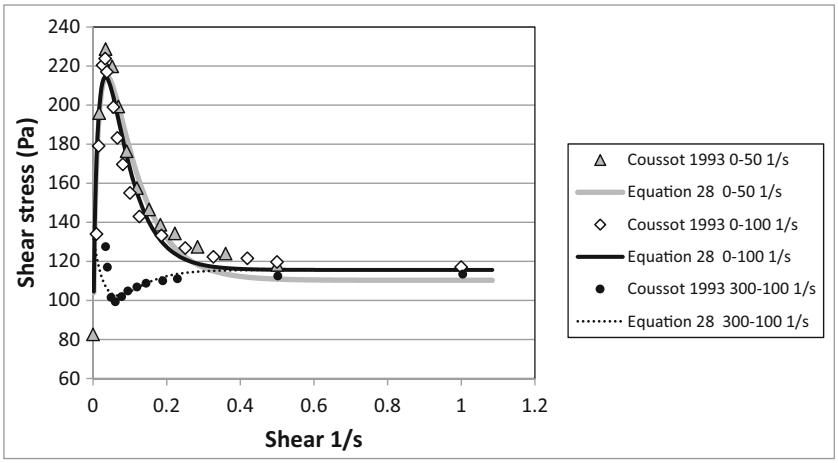

Fig. 7 Comparison of changes in shear stress in response to step-up (0–50 and 0–100 s^{-1}) and step-down (300–100 s^{-1}) experiments using bentonite from Coussot (1993)

Equation 28 was applied in a straight forward upwind fashion with the shear stress at time t_{i+1} calculated on the basis of the values of γ, λ_e and λ at time t_i. The convergence of $\lambda \rightarrow \lambda_e$ was calculated using Eq. 2. The time step used was 2×10^{-3} s, and the model prediction and measured data were compared over the duration of a second.

Figure 7 shows a comparison of the predicted and measured between start-up flow of the bentonite mixture, increasing the shear of the mixture from zero to 100 s^{-1} and from zero to 50 s^{-1} and a comparison of the predicted and measured between sudden reduction in shear of the bentonite mixture, reducing the shear of the mixture from 300 to 100 s^{-1}. The rheological parameters used for the comparisons in Fig. 6 are given in Table 3. Additional parameters are $\mu_\infty = 0.064$ Pa. A dynamic yield stress of 103 Pa s was derived based on a fit of Eq. 28 to the equilibrium data provided in the Coussot (1993) paper. As in Toorman (1997), who modelled the same data using a Bingham approach, it was assumed that the rotation speed of the shearing apparatus takes a finite time to adjust. The adjustment to the new shear is assumed to be $\gamma = \gamma_2 + (\gamma_1 - \gamma_2)e^{-\alpha t}$ with $\alpha = 0.03$. The adjustment to the near shear is 99% complete within the first 0.15 s.

The step-up tests show an initial increase in shear stress resulting from the sudden increase in shear rate and the reduction in the equilibrium value of the structural parameter λ_e compared to the time-dependent value λ. This causes an increase in the yield strength $\tau_y = \left(\frac{\lambda}{\lambda_e}\right)\tau_0$ which causes the shear stress to increase. As $\lambda \longrightarrow \lambda_e$, then $\tau_y \longrightarrow \tau_0$, and the shear stress reduces in consequence. For the step-up tests, the situation is similar, but $\tau_y = \left(\frac{\lambda}{\lambda_e}\right)\tau_0$ initially reduces before slowly increasing as $\lambda \longrightarrow \lambda_e$.

Table 3 Rheological constants used to fit Eq. 28 in Fig. 7

D	$1/(4-D)$	m	a	β	τ_0 (Pa)
2.9	0.9	0.4	0.3	8	103

The results indicate that Eq. 28 performs well in reproducing the behaviour of clay suspensions in non-equilibrium conditions. The model performance does not require representation of different stationary and dynamic yield stress to reproduce the observations.

7.4 Step-up tests by Dullaert and Mewis (2006)

In this section, Eq. 28 is compared against step-up shear (and equilibrium) experiments from Dullaert and Mewis (2006). This is a test of the model on a clay-like but non-aqueous colloidal suspensions. The suspension in the measurements was composed of fumed silica particles, dispersed in a Newtonian mixture of paraffin oil and 27.5 vol% PIB. The viscosity of the suspending fluid was 0.65 Pa s. Equation 28 was applied as in Sect. 6.3. The convergence of $\lambda \rightarrow \lambda_e$ was calculated using Eq. 7. The time step used was 2×10^{-2} s, and the model prediction and measured data were compared over the duration of 100 s. Figure 8 shows a comparison of the predicted and measured between start-up flow of the flumed silica slurry, increasing the shear of the mixture from 0.1 to 5 s^{-1}, from 0.1 to 2.5 s^{-1}, from 0.1 to 1.0 s^{-1}, from 0.1 to 0.5 s^{-1} and from 0.1 to 0.25 s^{-1}. The rheological parameters used for the comparisons in Fig. 6 are given in Table 4. Additional parameters are $\mu_\infty = 0.078$ Pa (calculated on the basis of Eq. 8 using the stated fluid viscosity of 0.065 Pa s (Dullaert and Mewis 2006) and an estimate of the maximum packing fraction of flumed silica of 0.33 (Mondragon et al. 2012).

Firstly, the equilibrium form of Eq. 28 (Eq. 29) is compared against the measured data (Fig. 8). These parameters are then used as a basis for the comparison of the time-dependent data in Fig. 9. The results indicate that Eq. 28 (and Eq. 29) performs adequately in reproducing the viscous behaviour of the flumed silica suspension in non-equilibrium conditions. However, as the model considered here is purely viscous, it is not able to reproduce the elastic behaviour noted by Dullaert

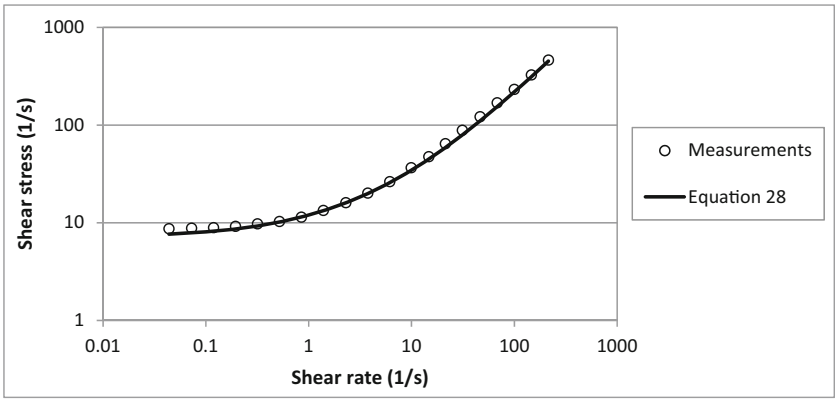

Fig. 8 Comparison of Eq. 29 with data using fumed silica from Dullaert and Mewis (2006)

and Mewis (the initial rise in shear stress for the smaller shear rates) that occurs over the first 0.1 s. Dullaert and Mewis (2006) were able to reproduce this effect by including a viscoelastic contribution to the stress.

8 Discussion

There are many aspects of the study of rheology, and different models can be useful under different circumstances for describing the rheology of a particular substance. In this paper, we consider the rheology of aqueous clays, and in particular with an interest in coastal situations where clay suspensions can be mobilised and can result in a range of shear and of suspension concentrations. For this area of study, rheological models need to be applicable across these ranges, and therefore, a greater understanding of the underlying dependence of the rheology is required than is currently afforded by rheological models in the literature. The more sophisticated rheological models available in the literature (see Sect. 3) are designed to reproduce the detail of rheological phenomena and have a large number of fitting parameters to facilitate this which have to be derived from laboratory measurements. Such models have greatly improved the understanding and prediction of the elastic-viscous regime transition, but, while the fitting of a large number of empirical parameters allows a specific rheology to be well reproduced, this not necessarily enable the rheology of a similar but more concentrated sediment solution might behave. Moreover, increasing model sophistication through increasing the number of model parameters tends to increase, rather than decrease, uncertainty in the model prediction (Hill et al. 2013).

Table 4 Rheological constants used to fit Eqs. 28 and 29 in Figs. 8 and 9

D	$1/(4-D)$	m	a	β	τ_0 (Pa)
2.3	0.6	0.36	0.1	7	7

The equation developed in this paper includes aspects of the physics inherent in clay flocculation. The new equation is shown to compare well with both equilibrium data across the range of shear and sediment concentration and with time-varying data for shear step-up and step-down experiments. However, the equation has limitations—in particular, it does not at present include an elastic component and therefore is unable to reproduce the full aspects of the elastic-viscous regime transition which has implications for phenomena such as avalanching and fluidisation.

The proposed model is composed of two equations: one governing the time dependence of the structural parameter (Eq. 28) and one governing the dependence of the shear stress on shear rate and the structural parameter (Eq. 7).

The proposed model depends on the following six parameters, of which five require estimation or tuning, depending on the circumstances. Each of these parameters is discussed, in turn, below.

D The fractal dimension may be measured, but it is more common that D is a tuning parameter and identified through best fit analysis. Measurement of the fractal dimension can be undertaken using a light scattering technique (e.g. using a Malvern Mastersizer 2000). The scattering vector $Q = \frac{4\pi\eta}{\chi} sin\left(\frac{\theta}{2}\right)$ is related to the intensity of scatted light via the relation $I(Q) \propto Q^{-D}$, and D can then be found from a double logarithmic plot of I against Q (Pignon et al. 1997; Amjad and Khan 2016). In this equation, η is the refractive index of the suspending medium, X is the wavelength of the radiation and θ is the scattering angle. The fractal index can also be derived using N_2 adsorption data (Aparicio et al. 2004). For dilute floc suspensions, video techniques can be used (Maggi 2007), but such video techniques are unlikely to work satisfactorily for dense suspensions.

Based on the fits to data in this study, D was most commonly found to have a value of around 2.3 (i.e. $\frac{1}{(4-D)} \sim 0.6$), but the Bentonite example in this study had a much higher value of around 2.9 ($\frac{1}{(4-D)} \sim 0.9$), and the Hendratta and Ohmoto example of kaolinite had a value of around 1.7

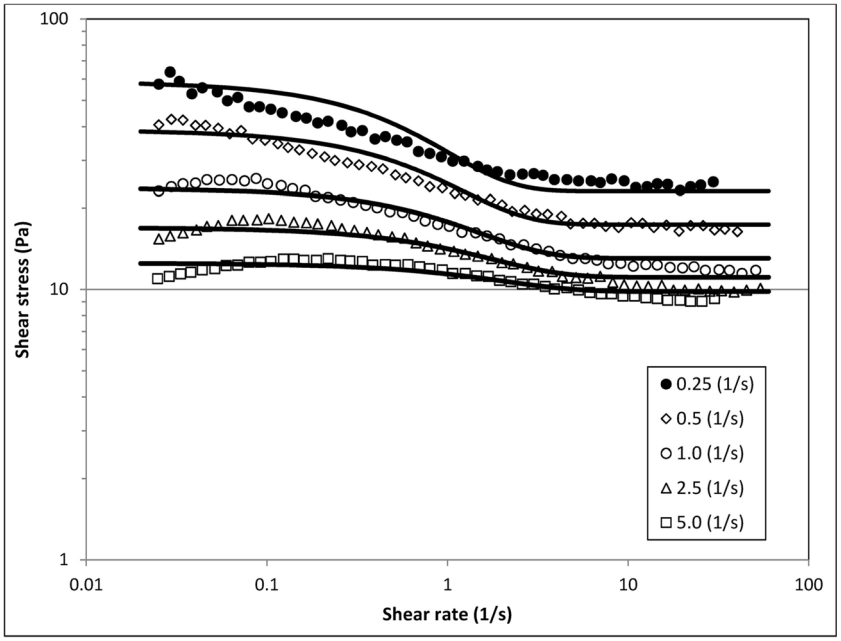

Fig. 9 Comparison of changes in shear stress in response to step-up (from 0.1 to 5 s^{-1}, to 2.5 s^{-1}, to 1.0 s^{-1}, to 0.5 s^{-1} and to 0.25 s^{-1}) experiments using fumed silica from Dullaert and Mewis (2006)

($\frac{1}{(4-D)}$~0.43). This range of values is typical of the range encountered in clay suspensions of the type considered in this paper.

As noted in Sect. 2 the fractal dimension is not strictly constant, and in practice, it reduces slowly with increasing floc size. It can therefore be expected that the fractal dimension reduces with increasing shear. The evidence shown in this paper suggests that in practice, this does not matter, but it may be necessary under some circumstances to include this variation.

m This is a parameter from the structural dependency equation (Eq. 28) which also appears in Eq. 29. It therefore affects both the rate at which the structural parameter approaches equilibrium and the rate at which the non-Newtonian effects on the shear stress decline with increasing shear. If the value of the fractal dimension is known, then m can be established from a plot like Fig. 3 since at low non-dimensional shear rates, the behaviour of $T = \tau/\tau_0$ is a power function of $\Gamma = \gamma/\gamma_0$ with an exponent of $\frac{1}{(4-D)} - m$ which is equal to the gradient of the double logarithmic plot. Otherwise, D and m are tuning parameters and identified through best fit (e.g. least squares) analysis.

The clays examined in this study exhibit a range of values of m varying from 0.001 through to 0.75. It is not surprising that the value of m varies with the type of clay, but it can also vary significantly for similar clays—as a comparison between the kaolinites studied by Coussot (1995) and Mondragon et al. (2012) shows. Bekkour et al. (2005) showed that the variation in the exponent m of the shear in the rate equation is partly a function of the sediment volume concentration. Further studies of the exponent m for different clays and conditions are required.

τ_0 τ_0 may be measured for a range of concentrations or for a few values but sufficient to identify the parameter c in $\tau_0 = k\left[\frac{\phi/\phi^*}{(1-\phi/\phi^*)}\right]^{2(4-D)}$, or τ_0 may be a tuning parameter.

μ_∞ This is the high shear limit of the viscosity and is calculated from $\mu_\infty = \mu_0\left[\frac{1}{(1-\phi/\phi^*)}\right]^2$

β This is a parameter from the structural dependency equation (λ_e in Eq. 28) which also appears in Eq. 29. It therefore affects both the rate at which the structural parameter approaches equilibrium and the rate at which the non-Newtonian effects on the shear stress decline with increasing shear rate. In practice, it is a tuning parameter and is identified through best fit (e.g. least squares) analysis. However, a guide to the value of β may be derived from a plot like Fig. 3. The intercept of the linear fit of the double logarithmic plot at low (non-dimensional) shear is approximately $ln\left[\frac{1}{\beta^{1/(4-D)}}(4-D)\right]$.

a This is an empirical parameter controlling the rate of convergence of the structural parameter to its equilibrium value. In practice, it is a tuning parameter and is identified through best fit analysis.

9 Conclusions

This paper establishes a framework for rheology of clay suspensions valid for the whole range of sediment concentrations and shear from the yield point to Newtonian flow. The shear stress equation is reconstructed from first principles of flocculation using an approach adapted from Mills and Snabre (1988). Structural kinetics theory (Moore 1959; Worrall and

Tuliani 1964) is then added to this equation. The derivation results in a rheology equation which is able to reproduce the behaviour of clay suspensions at low and high shear, incorporates the dependence of yield strength and viscosity on clay volume concentration, reproduces the effects of time-dependent structural changes on rheology and is compatible both with the form of structural similarity highlighted by Coussot (1995). The new equation is shown to compare well with both equilibrium data across the range of shear and sediment concentration and with time-varying data for shear step-up and step-down experiments. Five tunable parameters are required to fit the model to data, depending on the information available. Inclusion of aspects of the physics inherent in clay flocculation, together with structural dynamics, allows the proposed rheological model to represent the breadth of clay suspension behaviour and appears to represent an improvement over the available rheological models of the viscous regime; although, as the model does not include an elastic rheology component, the model is not able to reproduce well the behaviour associated with the elastic-viscous transition.

References

Alexandrou AN, Constantinou N, Georgiou G (2009) Shear rejuvenation, aging and shear banding in yield stress fluids. J Non-Newtonian Fluid Mech 158:6–17

Amjad H, Khan Z (2016) A comparison of fractal dimensions of clay and humic acid flocs under optimum coagulation conditions. In J Environ Sci Dev 7(4):240–243

Aparicio P, Pérez-Bernal JL, Galán E, Bello MA (2004) Kaolin fractal dimension: comparison with other properties. Clay Miner 39:750–784

Armelin E, Martí M, Rudé E, Alemán C (2006) A simple model to describe the thixotropic behavior of paints. Progress in Organic Coatings 57(3):229–235

Armstrong MJ, Beris AN, Rogers SA, Wagner NJ (2016) Dynamic shear rheology of a thixotropic suspension: comparison of an improved structure-based model with large amplitude oscillatory shear experiments. J Rheol 60:433–450

Bache DH, Gregory R (2007) Flocs in water treatment. IWA Publishing, London

Bekkour K, Leyama M, Benchabane A, Scivener O (2005) Time-dependent rheological behaviour of bentonite suspensions. J Rheol 49(6):1329–1345

Berlamont J, Ockenden M, Toorman E, Winterwerp J (1993) The characterisation of cohesive sediment properties. Coast Eng 21:105–128

Blachier C, Jacquet A, Mosquet M, Michot L, Baravian C (2013) Impact of claymineral particle morphology on the rheological properties of dispersions: a combined X-ray scattering, transmission electronic microscopy and flow rheology study. Appl Clay Sci 87:87–96

Blackwell B C (2013) Thixotropic-viscoelastic rheological fingerprints in large amplitude oscillatory shear, Masters Thesis for the University Illinois, 2013

Bremer L G B (1992) Fractal aggregation in relation to formation and properties of particle gels, PhD Thesis for the University of Wageningen, 1992

Chong JS, Christiansen EB, Baer AD (1971) Rheology of concentrated suspensions. J Appl Polym Sci 15:2007–2021

Coupland JN and Sigfusson H (2006) Food emulsions, In: (Ed) Yiu H Hui, Handbook of Food Science, Technology, and Engineering, Volume 3, 138–1 to 138–11

Coussot P (1993) Rheology of concentrated dispersed systems in a low molecular weight matrix. J Non-Newtonian Fluid Mech 46:179–211

Coussot P (1995) Structural similarity and transition from Newtonian to non-Newtonian behavior for clay-water suspensions. Phys Rev Lett 74(20):3971–3974

Coussot P, Nguyen QD, Huynh HT, Bonn D (2002) Avalanche behavior in yield stress fluids. Phys Rev Lett 88(17):175501-1–175501-4

Derjaguin B, Muller V, Toporov Y (1975) Effect of contact deformations on the adhesion of particles. J Colloid Interface Sci 53:314

Dullaert K, Mewis J (2006) A structural kinetics model for thixotropy. J Non-Newtonian Fluid Mech 139:21–30

Firth BA, Hunter RJ (1976) Flow properties of coagulated colloidal suspensions: III the elastic floc model. J Colloid Interface Sci 57(2): 266–275

Galindo-Rosale FJ, Rubio-Hernández FJ (2006) Structural breakdown and build-up in bentonite dispersions. Appl Clay Sci 33:109–115

Genovese DB (2012) Shear rheology of hard-sphere, dispersed and aggregated suspensions and filler-matric composites. Adv Colloid Interf Sci. 171–172:1–16

Gratiot N and Manning A J (2008) Flocculation processes in concentrated benthic suspension layer using a laboratory diffusive turbulent grid tank, In: T Kusuda, Y Hiroyuki, J Spearman, J Z Gailani (eds), Sediment and Ecohydraulics: INTERCOH 2005, Elsevier, Amsterdam.

Hammadi L, Boundjenane N, Houdjedje R, Reffis R, Belhadri M (2015) Modeling the time-dependent rheological behaviour of clays used in fabrication of ceramic, International Journal of Mechanical, Aerospace, Industrial. Mechatronic and Manufacturing Engineering 9(7):1373–1376

Hendratta LA and Ohmoto T (2012) Non-newtonian properties and flow structure in hyper-concentrated sediment laden flows, Annals of Faculty Engineering Hunedoara - International Journal ofd Engineering, Tome X, Fascicule 3, ISSN 1584-2673, 57–62

Hill L J, Sparks R S J and Rougier J C (2013) Risk assessment and uncertainty in natural hazards, In: J Rougier, S Sparks and L Hill (eds), Risk and Uncertainty Assessment for Natural Hazards, Cambridge University Press

Huang H (1993) Porosity-size relationship of drilling mud flocs: fractal structure. Clay and Clay Minerals 41(3):373–379

van Kessel T (1996) Rheological properties of cohesive sediment suspensions, report no. 1–96, Technical University of Delft, March 1996.

Khelifa A and Hill PS (2006) Models for effective density and settling velocity of flocs. J Hydraul Res 44(3):390–401

Knoch D and Malcherek A (2011) A numerical model for simulation of fluid mud with different rheological behaviors, Ocean Dynamics;Mar2011, Vol. 61 Issue 2/3, p245.

Krieger IM and Dougherty T J (1959) A mechanism for non-Newtonian flow in suspensions of rigid spheres. Trans. Soc. Rheol., III:137–152

Maggi F (2005) Flocculation dynamics of cohesive sediment. Doctoral Thesis for the Technical, University of Delft

Maggi F (2007) Variable fractal dimension: a major control for floc structure and flocculation kinemativs of suspended cohesive sediment. J Geophys Res 112(C7). doi:10.1029/2006JC003951

Manning A J, Baugh J V, Spearman J and Whitehouse R J S (2011) Cohesive sediment flocculation and the application to settling flux modelling, In: Sediment transport. Intech, Vienna, Austria. http://www.intechopen.com/books/sediment-transport/cohesive-

sediment-flocculation-and-the-application-to-settling-flux-modelling
Markussen TN and Andersen TJ (2013) A simple method for calculating in situ floc settling velocities based on effective density functions. Mar Geol 344:10–18
McClements DK (1999) Food emulsions, principles, practice and technique. CRC Press LLC, London
Metin CO, Bonnecaze RT, Lake LW, Miranda CR, Nguyen QP (2014) Aggregation kinetics and shear rheology of aqueous silica suspensions. Appl Nanosci 4(2):169–178
Mills P (1985) Non-newtonian behaviour of floc suspensions. J Physique Lett 46:301–409
Mills P and Snabre P (1988). The fractal concept in the rheology of concentrated suspensions, p.105–108. In: Giesekus H. et al. (Eds.). Progress and Trends in Rheology II, Springer-Verlag Berlin, Heidelberg
Moller P, Fall A, Chikkadi V, Derks D, Bonn D (2009) An attempt to categorize yield stress fluid behaviour. Phil Trans R Soc A 367: 5139–5155
Møller PCF, Mewis J, Bonn D (2006) Yield stress and thixotropy: on the difficulty of measuring yield stresses in practice. Soft Matter 2:274–283
Mondragon R, Julià JE, Barba A, Jarque JC (2012) Determination of the packing fraction of silica nano particles from the rheological and viscoelastic measurements of nanofluids. Chem Eng Sci 80:119–127
Moore F (1959) The rheology of ceramic slips and bodies. Trans Brit Ceramic Soc 58:470–494
Oberrecht D, Wurpts A (2014) Investigations of rheological flow properties based on lab data of fluid mud samples and an extended model approach. Die Küste 8:455–462
Pignon F, Magnin A, Piau J-M, Cabane B, Lindner P, Diat O (1997) Yield stress thixotropic clay suspension: investigations of structure by light, neutron, and x-ray scattering, Physical Review E. Volume 56(3):3281–3289
Pignon F, Magnin A, Piau J-M (1998) Structure under shear flow of thixotropic clay gels, proceedings of SASFLOW '98, may 1998. Grenoble, France
Quemada D (1977) Rheology of concentrated disperse systems and minimum energy dissipation principle—I. Viscosity concentration relationship. Rheologica Acta 16(82–94):1977
Quemada D (1998) Rheological modelling of complex fluids: I. The concept of effective volume fraction revisited. Eur Phys J AP 1: 119–127
Snabre P, Bitbol M, Mills P (1987) Cell disaggregation behaviour in shear flow. J Biophys 51:795–807
de Souza MPR (2011) Thixotropic elasto-viscoplastic model for structured fluids. Soft Matter 7:2471–2483
de Souza MPR, Thompson RL (2013) A unified approach to model elasto-viscoplastic thixotropic yield stress materials and apparent yield stress fluids. Rheol Acta 52(7):673–694
Toorman E (1997) Modelling the thixotropic behaviour of dense cohesive sediment suspensions. Rheol Acta 36:56–65
Van Olphen H (1956) Forces between suspended bentonite particles, clays and clay minerals, Natl. Acad.Sci., Natl.Res.Coun.pub., 2040224.
Willenbacher N and Georgieva K (2013) Rheology of disperse systems, In: Product Design and Engineering: Formulation of Gels and Pastes, Wiley-VCH Verlag GmbH and Co, 2013
Winterwerp JC, van Kesteren WGM (2004) Introduction to the physics of cohesive sediment in marine environment. Elsevier, New York
Worrall WE, Tuliani S (1964) Viscosity changes during the ageing of clay-water suspensions. Trans Brit Ceramic Soc 63:167–185
Xu C and Dong P (2016) A dynamic model for coastal mud flocs with distributed fractal dimension, Journal of Coastal Research, http://www.jcronline.org/doi/pdf/10.2112/JCOASTRES-D-15-00110.1. Accessed 1 Nov 2016
Zhou Z, Solomon MJ, Scales PJ, Bodger DV (1999) The yield stress of concentrated flocculated suspensions of size distributed particles. J Rheol 43:651–671